Published in final edited form as:
Neuron. 2006 May 4; 50(3): 377–388. doi:10.1016/j.neuron.2006.03.023.

Pten Regulates Neuronal Arborization and Social Interaction in Mice

Chang-Hyuk Kwon[1,3,4], **Bryan W. Luikart**[1,4], **Craig M. Powell**[2,4], **Jing Zhou**[1], **Sharon A. Matheny**[1], **Wei Zhang**[1], **Yanjiao Li**[1], **Suzanne J. Baker**[3], and **Luis F. Parada**[1,*]

[1]Center for Developmental Biology and Kent Waldrep Foundation Center for Basic Neuroscience Research on Nerve Growth and Regeneration

[2]Departments of Neurology and Psychiatry, University of Texas Southwestern Medical Center, Dallas, Texas 75390

[3]Department of Developmental Neurobiology, St. Jude Children's Research Hospital, Memphis, Tennessee 38105

Summary

CNS deletion of *Pten* in the mouse has revealed its roles in controlling cell size and number, thus providing compelling etiology for macrocephaly and Lhermitte-Duclos disease. *PTEN* mutations in individuals with autism spectrum disorders (ASD) have also been reported, although a causal link between PTEN and ASD remains unclear. In the present study, we deleted *Pten* in limited differentiated neuronal populations in the cerebral cortex and hippocampus of mice. Resulting mutant mice showed abnormal social interaction and exaggerated responses to sensory stimuli. We observed macrocephaly and neuronal hypertrophy, including hypertrophic and ectopic dendrites and axonal tracts with increased synapses. This abnormal morphology was associated with activation of the Akt/mTor/S6k pathway and inactivation of Gsk3β. Thus, our data suggest that abnormal activation of the PI3K/AKT pathway in specific neuronal populations can underlie macrocephaly and behavioral abnormalities reminiscent of certain features of human ASD.

Introduction

Phosphatase and tensin homolog on chromosome ten (*PTEN*) is a tumor suppressor gene mutated in many human cancers (Ali et al., 1999). Individuals with germline *PTEN* mutations are prone to tumors but also display brain disorders, including macrocephaly, seizure, Lhermitte-Duclos disease, and mental retardation (Waite and Eng, 2002). *PTEN* mutations also have been reported in autistic individuals with macrocephaly (Butler et al., 2005;Goffin et al., 2001;Zori et al., 1998).

PTEN has lipid phosphatase activity against the 3′ phosphate of phosphatidylinositol 3,4,5 trisphosphate (Maehama and Dixon, 1998). Phosphatidylinositol 3-kinase (PI3K) catalyzes the reverse of this reaction, resulting in AKT activation. Upon activation, AKT phosphorylates a diverse spectrum of substrates, including *tuberous sclerosis complex 2* (*TSC2*) gene product tuberin, glycogen synthase kinase 3β (GSK3β), and the proapoptotic protein BAD (Luo et al., 2003).

*Correspondence: luis.parada@utsouthwestern.edu.
[4]These authors contributed equally to this work.

Supplemental Data
he Supplemental Data for this article can be found online at http://www.neuron.org/cgi/content/full/50/3/377/DC1/.

Abnormalities in many components of the PI3K/AKT pathway have been associated with diverse brain disorders. For example, inactivating mutations in *PTEN* or activating mutations in *PI3K* are found in malignant brain tumors (Ali et al., 1999;Broderick et al., 2004), low AKT level is associated with schizophrenia (Emamian et al., 2004), and individuals with *TSC* mutations have CNS disorders, including autism (Wiznitzer, 2004). The PI3K/AKT pathway has also been linked to activity-dependent plasticity processes in the brain. Activation of the pathway was found in the amygdala in fear-conditioned rats (Lin et al., 2001). Components of the mTOR/S6K pathway, downstream of PI3K/Akt, are present in synapses and mediate synaptic plasticity through local protein synthesis (Tang et al., 2002).

Pten null mice die during embryogenesis, and heterozygotes are prone to tumors in the prostate, endometrium, and lymphoid system (Stiles et al., 2004). Conditional loss of *Pten* can have differing consequences depending on the cell type or its state of differentiation. Consistent with the frequent association of somatic mutations with cancer, *Pten* deletion in dividing T-lymphocytes, mammary epithelial cells, neural stem cells, and astrocytes induced hyperplasia (Fraser et al., 2004;Groszer et al., 2001;Li et al., 2002;Suzuki et al., 2001). *Pten* deletion in granule neurons, cardiomyocytes, and the cerebellum induced cellular hypertrophy (Crackower et al., 2002;Kwon et al., 2001). In primary neuron cultures, the PI3K pathway regulates cell survival, neurite growth, and dendritic arborization (Crowder and Freeman, 1998;Jaworski et al., 2005;Klesse and Parada, 1998;Markus et al., 2002). The above studies manipulated either mitotic cells or immature neurons. The in vivo role of the PI3K/PTEN/AKT pathway has been poorly studied in mature neurons where specialized properties including synapses and polarity are already established.

In the present study, we employed a *Neuron-specific enolase* (*Nse*) promoter-driven *cre* transgenic mouse line, in which cre activity is confined to discrete mature neuronal populations in the cerebral cortex and hippocampus (Kwon et al., 2006). The resulting conditional *Pten* mutant mice develop macrocephaly due to crespecific neuronal hypertrophy. We identified abnormal dendritic and axonal growth and synapse number. The mice exhibit altered social behavior and inappropriate responses to sensory stimuli.

Results

Pten Is Inactivated in Differentiated Neurons

Cre activity in the brain of *Nse-cre* mice was limited to subsets of differentiated neurons, mostly in layers III to V of the cerebral cortex and in the CA3, dentate gyrus granular layer (GL), and polymorphic layer (PML) of the hippocampal formation (Kwon et al., 2006). By 4 weeks of age, roughly 30%–60% of the neurons in these regions expressed functional β-galactosidase when crossed with *Rosa26-stop-lacZ* cre reporter (*Rosa26R* hereafter) (Soriano, 1999). A low level of sporadic cre activity was observed in a few neurons in the olfactory bulb, spinal cord, and cerebellar Purkinje cell layer. To confirm cre activity in differentiated neurons, we stained brain sections from 2-week-old mice for β-galactosidase and either a dendritic marker, microtubule-associated protein-2 (MAP2), or a neural stem cell marker, nestin. In the dentate gyrus at this age, active neurogenesis is still occurring in the subgranular zone (SGZ) between the GL and the PML (Shapiro and Ribak, 2005). Most granule neurons in the dentate gyrus are born in the SGZ and migrate and differentiate outward into the GL. In *Nse-cre; Rosa26R* brains, β-galactosidase colocalized with MAP2-expressing cells in the outer GL and the PML, but not in the inner GL or the SGZ. No β-galactosidase was detected in nestin-positive cells (Figure 1A). Consistent with this, postnatal day 15 (P15) *Nse-cre; Rosa26R* brains pulsed with bromodeoxyuridine (BrdU) at P14 did not show colocalization of BrdU and β-galactosidase (Figure 1B), indicating the absence of cre activity in dividing neuronal precursors. Chasing BrdU signal 4 weeks after

the pulse revealed partial colocalization of BrdU and β-galactosidase in dentate granule neurons. Thus, cre activity is confined to subsets of differentiated neurons in *Nse-cre* mice.

Nse-cre; Pten$^{loxP/loxP}$ mice (mutant mice hereafter) were viable at birth and appeared normal until 4–5 weeks of age. Consistent with a previous report (Perandones et al., 2004), control mice showed Pten signal in most differentiated neurons, including those in the GL and PML of the dentate gyrus and cerebral cortex (Figures 1C and 1D, respectively). At 2 weeks of age, mutant dentate gyrus exhibited Pten-negative cells at the PML and the outer GL, similar to the cre activity of *Nse-cre; Rosa26R* brains. The same regions also showed increased phospho-Ser473-Akt (P-Akt), a marker for Akt activation. At 4 weeks of age, Pten-negative and PAkt-positive cells increased in mutant dentate GL, indicating that *Pten* deletion accompanies differentiation of dentate granule neurons. *Pten* deletion and increased P-Akt signal were found in all sites of Nse-cre activity (Kwon et al., 2006), and the ratios of *Pten* deletion (55.89% ± 6.62% in dentate granule neurons; 44.88 ± 1.62% in sensory cortical layers III to V) coincided with the ratios predicted by the *Rosa26R* assays, indicating similar recombination efficiency for the *loxP-Pten* and *Rosa26* alleles.

Behavioral Abnormalities in Social Interaction and Social Learning

Autistic spectrum disorders (ASD) have been reported in individuals with germline *PTEN* mutations (Butler et al., 2005;Goffin et al., 2001;Zori et al., 1998). Since the adult *Pten* mutant mice tended to be isolated from their littermates within the cage, we examined the colony using a series of established behavioral paradigms. We found that mutant mice exhibit a distinct pattern of behavioral abnormalities reminiscent of ASD.

Mice are a social species and display behavioral social interaction (Murcia et al., 2005). Thus, social interaction and nesting have been proposed as core paradigms to test autistic behavior in mice (Crawley, 2004) and have been used to measure autism-like behaviors in other mutant mouse models (Lijam et al., 1997;Moretti et al., 2005). As anticipated, control mice exposed to a novel conspecific juvenile exhibited typical behavior of approaching and sniffing, but such initial social interaction was profoundly decreased in mutant mice (Figure 2A). When re-exposed to the same juvenile after 3 days, control mice exhibited a typical decrease in social interaction compared to the initial interaction, indicating recognition of the familiar juvenile and normal social learning. The mutant mice, however, did not decrease their interaction, indicating impaired social learning or inability to identify the juvenile due to the low level of initial interaction. We next examined nest formation, a test for home cage behavior (Lijam et al., 1997;Moretti et al., 2005). In contrast to the immediate activity of nest formation in control mice, mutant mice showed little nest-forming activity (Figure 2B). We do not attribute the abnormalities in social interaction and nest formation to deficiencies in general interest in novelty or olfactory sensation, since we did not detect significant difference between groups in tests for novel inanimate object interaction (Figure 2C) or olfaction (Figure 2D). Each of the above tests was fully replicated with equivalent significant results using a separate cohort of mice and performed by a different investigator, demonstrating the reproducibility of the results (data not shown).

Additional social tests gave similar results. For example, another social interaction test presents a test mouse with a caged adult mouse (social target) and an empty cage (inanimate target) in an open field. Control mice spent significantly more time interacting with the social target than with the inanimate target (Figure 2E). In contrast, *Pten* mutants showed decreased interaction with the social target compared to controls and spent a similar amount of time interacting with both targets. Another test for social novelty uses a three-roomed chamber. Initial interaction with the empty cage was similar in both groups, while interaction with the social target was significantly decreased in mutants compared to controls (Figure 2F). Subsequently, when mice were exposed to the familiar mouse versus a

novel mouse, control mice showed a clear preference for the novel mouse over the familiar mouse as expected, while mutant mice did not show a preference for social novelty (Figure 2G). Additionally, mutants showed significantly less interaction with the novel target mouse compared to controls. In summary, the mutant mice exhibited decreased social interaction without change in novel object exploration or a preference for social novelty. Thus, the *Pten*-deficient mice display deficiencies in classic social interaction paradigms.

We also measured sexual and maternal behavior. While all naive control males made female mice pregnant, none of naive mutant males did. Although we do not exclude potential reproductive defects, we did not observe any active sexual behavior, such as mounting, from the mutant males. While mutant females could be fertilized by normal males, mortality of pups by P5 was higher than control group (Figure 2H), indicating defects in maternal care. Taken together, the *Pten* mutant mice exhibited abnormalities in social interaction, memory and preference, sexual behaviors, and maternal care in several different social paradigms.

Behavioral Abnormalities in Response to Sensory Stimuli, Anxiety, and Learning

By 6 weeks of age, mutant mice were also distinguishable from control mice in their response to novel sensory stimulation. When investigators handled mutant mice, they were unusually resistant to handling (n = 52). Consistent with this subjective observation, mutant mice exhibited normal locomotor activity in less stressful environments but hyperactivity under more stressful conditions. In the bright environment of the open field, mutants were hyperactive, traveling further (Figure 3A) at an increased average speed. However, in the dark/light boxes and in the enclosed, darker environments of the locomotor apparatus, locomotor activity was normal (see Figures S1A and S1B in the Supplemental Data available online). Additionally, mutants exhibited increased initial startle responses to a 120 dB white noise stimulus (Figure 3B). Upon repeated startle stimulation, mutants showed similar startle responses to controls, indicating normal habituation (Figure S1C). Sensorimotor gating, as measured with a prepulse inhibition paradigm, was also significantly impaired in mutant mice (Figure 3C). Thus, the mutants showed quantifiably increased activity in response to sensory stimuli.

Consistent with exaggerated response to stressful sensory stimuli, mutant mice also showed increased anxiety-like behavior in the open field test where they spent significantly less time in the center zone (Figure 3D) as well as a lower ratio of center versus periphery time (data not shown, $p = 0.02$). Similarly, in the dark/light apparatus, mutants showed longer latencies to enter the light side, spending the majority of their time on the dark side (Figure 3E). In a third anxiety-related test, the elevated plus maze, mutants did not show the increased anxiety-like behavior (Figure 3F). Indeed, there was an opposite effect in both the time spent in the open arms and the ratio of open arm entries to total arm entries (data not shown).

Because of the profound abnormalities in the dentate gyrus (described below), we tested the *Pten* mutant mice in the Morris water maze. Because of the abnormal anxiety, we habituated the mice to swimming in the maze for 4 days using a visible platform task. Mutant mice learned the visible platform task as well as controls, though there was a trend toward slower acquisition (Figure S1D). In the submerged platform version, measuring both latency to reach the platform and distance traveled to reach the platform, mutant mice did not learn as quickly as controls (Figure 3G). On the probe trial, control mice spent significantly more time in the target quadrant than the opposite quadrant, while mutants showed no significant preference (Figure 3H). In addition, mutant mice exhibited a significantly greater tendency to swim along the edge of the maze (thigmotaxis) (Figure 3I), which is similar to their behavior in the open field test.

In addition to the behavioral abnormalities described, 6 of 52 mutant mice studied, including 3 of 12 during the water maze test, showed sporadic seizures (subjective observation). Further analysis using electroencephalogram/electromyogram (EEG/EMG) recording revealed that all mutant mice analyzed (n = 3) developed spontaneous seizures during the light phase, but no seizures were observed in any of control mice (Table S1). Repetitive spike-wave patterns were noted, sometimes accompanied by rhythmic slow activity. Continuous spike-wave bursting could also be seen. The incidence of seizures was 0.67 per mouse per day, and the mean duration was 10 min 50 s. Sound and tactile stimuli did not induce seizures in any mouse (data not shown). The relatively low incidence and short duration of seizure recorded in the subset of mutant mice is consistent with the low frequency by subjective observation. Given the relatively low incidence and short duration of seizures, it is unlikely that seizures bear on the robust behavioral abnormalities seen in all 52 mice. Consistent with this view, as described below, mutant mice did not show any deficit in tests for locomotor activity and strength. In the accelerating rotarod test, mutant mice exhibited normal coordination during the initial trials (Figure S1E). Interestingly, while both groups showed significant motor learning, during subsequent rotarod trials, mutant mice actually performed better on this repetitive test of motor coordination compared to controls. In vertical pole and dowel tests to measure strength and endurance, mutant mice performed as well as controls (Figures S1F and S1G). In addition, mutant mice did not show deficits in context- and cue-dependent fear conditioning (Figure S1H).

Progressive Macrocephaly and Soma Hypertrophy in Mutant Brain

Mousestrains with broad neuronal *Pten* deletion showed somahypertrophy, macrocephaly, and premature death, occasionally with reduced body weight (Kwon et al., 2001, and unpublished observations). In the present study, the mutant mice appear to have a normal life span, presumably due to more restricted *Pten* deletion in subsets of postmitotic neurons. They also showed progressive macrocephaly, but without significant change in body weight (Figure 4A). The progressive macrocephaly was confined to the forebrain (cortex and hippocampus; Figures 4B and 4C), where most cre-mediated *Pten* deletion occurs (Kwon et al., 2006). Analysis of aging mice indicated eventual foliation of the DG and compression of the CA1 region (Figure 4C; lower right panel). Most dentate gyrus granule cells from wild-type mice expressed Pten and sustain relatively even soma diameter (Figure S2A). In contrast, Pten-negative neurons were larger than Pten-positive neurons at 4 weeks of age. The progressive increase in soma diameter and disorganized GL continued in mutant aging mice (Figures S2A and S2B). Such soma hypertrophy was also observed in the cortex and CA3 (Figure S2C) where cre activity is also present.

Regulation of Axonal Growth In Vivo

The Pten pathway is known to regulate neurite outgrowth in cell culture (Markus et al., 2002). Since *Nsecre* drives *Pten* ablation only in differentiated neurons with established polarity, we examined the effects of Pten loss on existing neuronal processes. In the dentate gyrus, granule neuron axons form the mossy fiber tract that projects from the GL through the PML to synapse with CA3 dendrites (Amaral, 1978). The extent of the mossy fiber tract was visualized by immunohistochemistry (IHC) using antibodies to synapsin I, a presynaptic marker, and to calbindin, which is expressed in the soma and processes of dentate granule neurons (Figure S3A). In adult mutants, the dentate gyrus showed a marked enlargement of the mossy fiber tract that progressed over time (Figures S3A and S3B). Confocal microscopy revealed that mutant axonal processes were more abundant and projected to a broader area (Figure 5A).

We also observed changes in the synapses of the mutant dentate gyrus. Synapsin I staining was increased in the inner molecular layer (ML) of aged mutants (arrows in Figure 5A).

Normally, most synapses in this region are derived from mossy cells of the PML and express calretinin (Blasco-Ibanez and Freund, 1997). The increased synapsin I staining of the inner ML did not completely overlap with calretinin staining (Figure S3C). Instead, the abnormally localized axonal projections appear to push mossy cell axons out of the inner ML. In fact, the abnormal axonal projections were positive for Timm's staining (Figure 5B), which is specific for the mossy fiber tract of the dentate gyrus (Danscher et al., 2004), demonstrating ectopic positioning of granule axons in the mutant mice.

Ultrastructural examination of the inner ML of mutant animals indicated a dramatic increase in presynaptic vesicle number compared to control animals (Figure 5C). In support of the Timm's staining data, the large vesicle pools were apposed to multiple postsynaptic densities, thus exhibiting the morphological appearance of granule neuron mossy fiber synapses in the CA3 region with characteristic enlarged presynaptic terminals. Taken together, these results suggest that Pten inactivation in differentiated neurons causes increased axonal growth, ectopic axonal projections, and abnormal synapses.

Regulation of Dendrite Growth and Spine Density In Vivo

To more closely examine the morphology of dendrites in mutant brains, we used Golgi staining. In the cerebral cortex from 3-month-old mutant mice, we observed thickened or elongated processes (Figure 6A). There was obvious dendritic hypertrophy in adult mutant dentate gyrus (Figure 6B). Estimation of the thickness of MAP2-positive dentate ML revealed a significant increase in mutants that progressed with age (Figure 6C). We also observed a 24.9% increase in dendritic spine density within the ML of mutant versus control mice (Figure 6C).

Ectopic neuronal processes extending from the cell bodies into the PML were observed in mutant dentate gyri at 3 months of age (data not shown) when the behavioral phenotypes were fully developed. The ectopic neuronal processes were thin and spiny but could not be unambiguously distinguished as dendrites or axons at this age. At 8 months of age, the ectopic neuronal processes in *Pten* null neurons extending into the PML were longer and thicker with obvious spines (arrows in Figures 6B and 7A). IHC for MAP2 revealed that the ectopic processes were molecularly discernable as dendrites at 10 months of age (Figure 7B). Double labeling for MAP2 and P-Akt showed a layer of ectopic dendrites between the GL and the PML with increased P-Akt in mutant dentate gyrus at 10 months of age. Furthermore, confocal images showed that most granule neurons displaying dendritic ectopia had increased P-Akt, while neurons lacking P-Akt signal did not display dendritic ectopia (Figure 7C), indicating that the ectopia was due to cellautonomous *Pten* deletion.

Molecular Correlates of Neuronal Hypertrophy and Abnormal Polarity

We next examined the status of downstream signaling components in *Pten*-deleted neurons. Previously, we reported that earlier *Pten* deletion in neurons increased P-Akt and phospho-Ser235/236-S6 (P-S6), markers for activation of the Akt and mTor/S6k pathways, respectively (Kwon et al., 2003). Here we show similar results when Pten is inactivated in differentiated neurons. We observed increased P-Akt and P-S6 in *Pten*-deleted, hypertrophic neurons, including the granule cells in the dentate gyrus at all ages tested (Figure 8A). Gsk3β is a direct target for Akt phosphorylation at Ser9, leading to functional inactivation (Cross et al., 1995). Both IHC and Western blot analysis demonstrate increased phospho-Ser9-Gsk3β (P-Gsk3β) in mutant tissues (Figure 8). Tuberin, the *Tsc2* product, is another direct target for Akt phosphorylation at Ser939 and an upstream regulator of the mTor/S6k pathway (Manning and Cantley, 2003). We detected increased phospho-Tuberin Ser939 (P-Tuberin) in the same tissues (Figure 8B). Thus, all tested downstream targets of Akt displayed increased phosphorylation in the *Pten*-deficient tissues.

Discussion

Through the use of cre-mediated recombination, we have deleted *Pten* and thus deregulated the PI3K pathway in subsets of differentiated neurons in the cortex and hippocampus.

Deregulation of Postmitotic Growth and Polarity of Neuronal Processes

At the time of *Pten* deletion, the dentate granule neurons already have established dendrites, extending over the full length of the ML, and axons projecting into the CA3 region. Furthermore, these neurons have already established synaptic connectivity. Our current findings indicate that Pten inactivation results in continued axonal and dendritic growth, with ectopic positioning of dentate axons to the ML and dendrites to the PML. Molecular markers for activation of the PI3K pathway were predictably detected. These data add to preceding reports of soma hypertrophy in *Pten*-deleted neurons (Backman et al., 2001;Kwon et al., 2001) and demonstrate that growth regulation by Pten extends to axons and dendrites.

Gsk3β was recently reported to be pivotal in controlling neuronal polarity in primary embryonic hippocampal neurons (Jiang et al., 2005;Yoshimura et al., 2005). In those studies, neurites destined to axons had more P-Gsk3β (inactive), and exogenous inactivation of Gsk3β resulted in formation of multiple axons. Conversely, expression of mutant Gsk3β insensitive to inactivation by Akt inhibited axon formation. Similar to the abnormal polarity in immature neurons, we observed hypertrophic axonal tracts and evidence of altered polarity of neuronal processes associated with inactivated Gsk3β in *Pten*-deleted, differentiated granule neurons. These results indicate that the PI3K/AKT/GSK3β pathway is critical not only for the establishment of polarity in undifferentiated neurons in culture but also for maintenance in differentiated neurons in vivo.

Behavioral Abnormalities in Social Interaction and Anxiety

In our mouse model, cre-mediated recombination affects subsets of differentiated neurons in the hippocampus and cerebral cortex. This process is reproducible, and the anatomical and behavioral phenotypes are robust and fully penetrant. The *Pten* mutant mice appear to have normal life span, which allowed us to test paradigms proposed for autistic behaviors in mice (Crawley, 2004). Indeed, the mutant mice exhibited deficits in all social paradigms tested and also showed exaggerated reaction to sensory stimuli, anxiety-like behaviors, seizures, and decreased learning, which are features associated with ASD (American Psychiatric Association, 2000). The elevated plus maze gave different results compared to open field and dark/light boxes. This may reflect different aspects of anxiety-like behaviors and their controlling neural networks (Dawson and Tricklebank, 1995). Nonetheless, two of three tests clearly showed anxiety-like behavior in the mutant mice. Normal behaviors in many paradigms, including locomotor, motor coordination, and fear conditioning, indicate that the mutant mice were not globally impaired. It is worth noting that the behavioral abnormalities of the mutant mice appeared at a time when morphological abnormalities were subtle (6 weeks of age).

A Potential Link with Autism

ASD is a neuropsychiatric disorder characterized primarily by deficits in social interaction and repetitive behaviors (Baron-Cohen and Belmonte, 2005). Many genetic factors have been implicated in ASD, including 15q11-q13 duplication and mutations responsible for fragile X mental retardation syndrome (*FMR1*) and Rett syndrome (Andres, 2002;Muhle et al., 2004). Intriguingly, a few neurological disorders related to one another by harboring mutations in the PI3K pathway are also atypically associated with ASD. Individuals with tuberous sclerosis have mutations in the *TSC1/2* complex and have a high incidence of ASD (25%–50%) (Asano et al., 2001;de Vries et al., 2005;Wiznitzer, 2004). In addition, the

incidence of ASD patients who are subsequently diagnosed with neurofibromatosis type 1 (NF1) greatly exceeds epidemiological prediction (Marui et al., 2004;Mbarek et al., 1999). Finally, the recent preliminary association of *PTEN* mutations in ASD with macrocephaly (Butler et al., 2005) further points to abnormal activation of the PI3K pathway as one possible etiology. NF1, PTEN, and the TSC complex are negative regulators of the PI3K pathway, and inactivation of any of the proteins results in a hyperactive signal transduction in many circumstances (Hay, 2005;Klesse and Parada, 1998;Manning and Cantley, 2003).

Diverse anatomical and cellular abnormalities have been reported in brains from ASD individuals. For example, both macrocephaly and microcephaly have been described in autistic individuals, with a ratio of 15% and 20%, respectively (Fombonne et al., 1999). Similarly, enlarged amygdala in children and enlarged hippocampus in children and adolescents have been associated with ASD (Schumann et al., 2004). The sum of recent findings seems to approach a consensus that increased brain volume is a relatively common feature of autism (Cody et al., 2002). There have also been reports in autism cases of enlarged or abnormally oriented neurons, densely packed neuronal regions and isolated regions of atrophic neurons with reduced dendritic arborization (Bauman and Kemper, 2005;Murcia et al., 2005). Thus, diverse genetic and cellular changes are present in autistic brains. It is important to emphasize that causal versus ancillary abnormalities remain to be rigorously determined (Baron-Cohen and Belmonte, 2005;Cody et al., 2002;Dakin and Frith, 2005).

Similar to our mouse model, mice null for *FMR1* displayed deficits in social and anxiety behaviors and increased spine density, which is also reported in fragile X syndrome (Bagni and Greenough, 2005). Both FMR1 and the mTOR/S6K pathway regulate protein translation and synaptic plasticity (Tang et al., 2002;Zalfa et al., 2003). Given the known association of fragile X syndrome in ASD (Andres, 2002), aberrant regulation of synaptic protein translation and abnormal synaptic connectivity may be a common theme affecting social interaction and anxiety in the mouse models and potentially in subsets of ASD as well. Conversely, in Rett Syndrome and some reports of autism, neuronal atrophy and reduced dendritic spines have been reported (Zoghbi, 2003). It may be possible that synaptic imbalance resulting from excess or reduced connectivity could result in the similar abnormalities found in ASD.

Experimental Procedures

Mice and Histology

Pten^{loxP} mice (Suzuki et al., 2001) were a gift from Tak Mak (University of Toronto), and *Rosa26R* mice were from Jackson Lab (Bar Harbor, ME). Tominimize transgenic variation due to genetic background, we maintained *Nse-cre; Rosa26R* or *Pten*^{loxP} mice in *C57/BL6* inbred background for at least three generations. For BrdU chasing, we injected subsets of 2-week-old *cre; Rosa26R* mice with BrdU as described (Fraser et al., 2004) and sacrificed them 1 day or 4 weeks after the injection. Mutant mice (*cre; Pten*$^{loxP/loxP}$) were born from breeding between *Pten*$^{loxP/loxP}$ mouse and *cre; Pten*$^{loxP/+}$ mouse or between *cre; Pten*$^{loxP/+}$ mice. Littermate controls used for this study were with a genotype of *cre; Pten*$^{+/+}$ or *Pten*^{loxP} mice without *cre*. For paraffin sectioning, we dissected out, processed, and sectioned brains as described (Fraser et al., 2004). For vibratome sectioning, we intracardially perfused the mice with ice-cold PBS followed by 4% (w/v) paraformaldehyde (PFA) in PBS. We dissected out the brain, post-fixed it in 4% PFA for overnight, and embedded it into 3% agarose. We made 50 μm thick coronal or horizontal sections by using a vibratome. All mouse protocols were approved by the Institutional Animal Care and Research Advisory Committee at University of Texas Southwestern Medical Center.

Immunostaining

We performed all IHC on triplicate sections per group. Based on anatomy, we chose matched sections from control and mutant. Antibodies used for IHC were against β-galactosidase (ICN, Aurora, OH), MAP2 (Sternberger Monoclonals, Lutherville, MA), nestin (BD Bioscience, San Jose, CA), BrdU (Dako, Carpinteria, CA), Pten (Neo-Markers, Winchester, MA), P-Akt, P-S6 (Cell Signaling, Beverly, MA), calbindin (Swant, Bellinzona, Switzerland), synapsin I, calretinin (Chemicon, Temecula, CA) or P-Gsk3β (Biosource, Camarillo, CA). For paraffin sections, we used microwave antigen retrieval for all antibodies, except that against P-Gsk3β. We visualized the primary antibodies by treating the sections with biotinylated secondary antibody and followed by amplification with peroxidase-conjugated avidin and DAB substrate. DAB-stained sections were counter-stained with hematoxylin or methyl green (Vector Labs, Burlingame, CA). Alternatively, we detected the primary antibodies by secondary antibodies conjugated with Cy3 (Jackson Immunoresearch, West Grove, PA) or Alexa Fluor 488 (Molecular Probe, Eugene, OR) followed by counterstaining with DAPI (Vector Labs).

Cell Counting, Size Measurement, Golgi Staining, and Electron Microscopy

To measure the ratio of *Pten* deletion, we counted Pten-positive or -negative neurons in a 7 × 5mm^2 area in the sensory cortex layers III to V and dentate GL by using MetaMorph software (Universal Imaging Corporation, West Chester, PA).We measured soma diameter of dentate granule neurons as described (Kwon et al., 2003), except for using the MetaMorph software. To estimate the length of the mossy fiber tract, we measured the center path of double-labeled signals for synapsin I and calbindin from the CA3 to the point at which two blades of dentate granular layer meet. Similarly, we estimated the thickest region of MAP2-positive dentate ML of either blade. We performed Golgi staining, image analysis, quantification of spine density, and electron microscopy as described (Luikart et al., 2005). Data were analyzed by Student's t test, except where noted, and displayed as mean ± SEM.

Behavioral Tests

Mutant mice were studied along with littermate controls in four cohorts of mice. Order of tests and cohorts are displayed in Table S2. Social interaction and social learning, interaction with a novel object, olfaction, strength tests by using vertical pole and dowel (Moretti et al., 2005), and nest formation (Lijam et al., 1997) were measured as described. Exceptions were performing social learning 3 days after the initial interaction test, placing one or two-mice per cage in nest formation, overnight food deprivation before olfaction test, and using Student's t test in strength tests. Caged social interaction for social versus inanimate target (Moy et al., 2004) was performed in a 48 × 48 cm^2 white plastic arena using two 6.0 × 9.5 cm rectangular cages of wire mesh with or without adult mouse, allowing olfactory and minimal tactile interaction. Social preference for novelty was performed as described (Moy et al., 2004), except room and door dimensions were different (15 × 90 × 18.5 cm divided into three rooms of 15 × 29 cm separated by dividers with a central 3.8 × 3.8 cm door), and video tracking software from Noldus (Ethovision 2.3.19) replaced photobeams and direct observation. In the test, mice were initially allowed to explore the room for 10 min. Then mice were allowed to interact with an empty cage in one room versus a caged social target in the far room. Subsequently, mice were allowed to interact with the familiar caged target mouse versus a novel caged target mouse. The open field test was performed for 10 min in a brightly lit (~800 lux), 48 × 48 cm^2 white plastic arena using video tracking software with a center zone defined as a 15 × 15 cm^2 square. Elevated plus maze, dark/light behavior, locomotor activity, accelerating rotarod, and Morris water maze were measured as described (Powell et al., 2004). Exceptions were scoring parameters by video tracking in elevated plus

maze and allowing each mouse three sets of three trials per day with ~10 min between trials and 3 hr between sets in accelerating rotarod test. A variation on the startle reflex and prepulse inhibition protocol (Dulawa and Geyer, 2000) was used. Mice were subjected to five pseudorandomly presented trial types in a 22 min session with an average of 15 s (7–23 s) between trials: Pulse alone (40 ms, 120 dB, white noise pulse), three different Prepulse/Pulse trials (20 ms prepulse of 4, 8, or 16 dB above background noise level of 70 dB precedes the 120 dB pulse by 100 ms, onset to onset), and no stimulus. Context and cue-dependent fear conditioning was performed as described (Powell et al., 2004), except a different plexiglass box with clear walls (MedAssociates) was used and two pairings of a 2 s, 0.8 mA footshock and tone were delivered with 60 s between pairings. Freezing behavior was monitored at 10 s intervals by an observer blind to the genotype. To measure sexual behavior, naive male mice (n = 4) were caged with two sexually experienced female mice up to 30 days. We observed their sexual behavior about 1 hr at the first day and 10 min at next 4 days. To measure maternal behavior, we mated one or two naive female mice with a sexually experienced male mouse up to 30 days. We counted pups at P0, P5, P10, and P15.

EEG/EMG Recording

Pten mutants (n = 3) and controls (n = 4) at 8–9 months of age were anesthetized and surgically implanted for long-term EEG/EMG monitoring as described (Chemelli et al., 1999). Mice were housed individually under a 12 hr light-dark cycle at 25°C, with food and water being replenished as necessary at CT 12:00 each day, but the mice were not otherwise disturbed. They were habituated to the recording conditions for 2 weeks before EEG/EMG signals were recorded over a period of 3 days, beginning at lights-off (CT 12:00). During the light period on the third day, sound and tactile stimuli were used to examine sensitivity to induced seizures. Mice were exposed to 10 min of an intense sound stimulus (a bunch of keys were shaken in the cage close to the mouse) followed by 3 min of tactile stimulus. Subsequently, the EEG/EMG record was visually screened for seizure epochs. Seizures were characterized as a spike-wave pattern on the EEG, typically accompanied by atonic periods or sustained rhythmic contractions on the EMG. Each seizure lasting for 2 s or more was noted.

Timm Staining

For Timm's staining, we intracardially perfused the mice with ice-cold 0.37% (w/v) sodium sulfide followed by 4% PFA. We dissected out the brain, postfixed it in 4% PFA for overnight, and cryoprotected in 30% (w/v) sucrose in PBS for 2–3 days. We made 16 μm thick coronal sections by using a cryostat. We performed a modified Timm staining as described (Danscher et al., 2004).

Western Blotting

We performed Western blotting as described (Kwon et al., 2003), except for loading 90 μg for P-Tuberin and Tuberin. Antibodies used for Western blotting were against Pten (NeoMarkers, Winchester, MA), P-Akt, P-S6, P-Gsk3β, P-Tuberin, Tuberin (Cell Signaling), or β-actin (Sigma, St. Louis, MO). We statistically analyzed chemiluminescence signals by using Kodak Image Station 2000R (Rochester, NY).

Supplementary Material

Refer to Web version on PubMed Central for supplementary material.

Acknowledgments

The authors thank Christopher Sinton and Shiori Ogawa for EEG/EMG analysis; Tak Mak for *Pten*^{loxP} mice; Junyuan Zhang, Xiaoyan Zhu, Steve McKinnon, Arash Khatami, Phillip Williams, David Theobald, Yajuan Liu, Ki-Woo Kim, and Jian Chen for technical assistance; and Gorm Danscher, Meredin Stoltenberg, Mark Lush, Douglas Benson, and Gary Westbrook for suggestions and helpful discussions. This work was supported in part by the American and Lebanese Associated Charities, NIH grant NS44172 (to S.J.B), and MH06597503 (to C.M.P.) NIH grant R37NS33199 and the American Cancer Society (to L.F.P.).

References

Ali IU, Schriml LM, Dean M. Mutational spectra of PTEN/MMAC1 gene: a tumor suppressor with lipid phosphatase activity. J. Natl. Cancer Inst. 1999; 91:1922–1932. [PubMed: 10564676]

Amaral DG. A Golgi study of cell types in the hilar region of the hippocampus in the rat. J. Comp. Neurol. 1978; 182:851–914. [PubMed: 730852]

American Psychiatric Association. Task Force on DMS-IV. Fourth edition. Washington DC: American Psychiatric Association; 2000.

Andres C. Molecular genetics and animal models in autistic disorder. Brain Res. Bull. 2002; 57:109–119. [PubMed: 11827743]

Asano E, Chugani DC, Muzik O, Behen M, Janisse J, Rothermel R, Mangner TJ, Chakraborty PK, Chugani HT. Autism in tuberous sclerosis complex is related to both cortical and subcortical dysfunction. Neurology. 2001; 57:1269–1277. [PubMed: 11591847]

Backman SA, Stambolic V, Suzuki A, Haight J, Elia A, Pretorius J, Tsao MS, Shannon P, Bolon B, Ivy GO, Mak TW. Deletion of Pten in mouse brain causes seizures, ataxia and defects in soma size resembling Lhermitte-Duclos disease. Nat. Genet. 2001; 29:396–403. [PubMed: 11726926]

Bagni C, Greenough WT. From mRNP trafficking to spine dysmorphogenesis: the roots of fragile X syndrome. Nat. Rev. Neurosci. 2005; 6:376–387. [PubMed: 15861180]

Baron-Cohen S, Belmonte MK. Autism: a window onto the development of the social and the analytic brain. Annu. Rev. Neurosci. 2005; 28:109–126. [PubMed: 16033325]

Bauman ML, Kemper TL. Neuroanatomic observations of the brain in autism: a review and future directions. Int. J. Dev. Neurosci. 2005; 23:183–187. [PubMed: 15749244]

Blasco-Ibanez JM, Freund TF. Distribution, ultrastructure, and connectivity of calretinin-immunoreactive mossy cells of the mouse dentate gyrus. Hippocampus. 1997; 7:307–320. [PubMed: 9228528]

Broderick DK, Di C, Parrett TJ, Samuels YR, Cummins JM, McLendon RE, Fults DW, Velculescu VE, Bigner DD, Yan H. Mutations of PIK3CA in anaplastic oligodendrogliomas, high-grade astrocytomas, and medulloblastomas. Cancer Res. 2004; 64:5048–5050. [PubMed: 15289301]

Butler MG, Dasouki MJ, Zhou XP, Talebizadeh Z, Brown M, Takahashi TN, Miles JH, Wang CH, Stratton R, Pilarski R, Eng C. Subset of individuals with autism spectrum disorders and extreme macrocephaly associated with germline PTEN tumour suppressor gene mutations. J. Med. Genet. 2005; 42:318–321. [PubMed: 15805158]

Chemelli RM, Willie JT, Sinton CM, Elmquist JK, Scammell T, Lee C, Richardson JA, Williams SC, Xiong Y, Kisanuki Y, et al. Narcolepsy in orexin knockout mice: molecular genetics of sleep regulation. Cell. 1999; 98:437–451. [PubMed: 10481909]

Cody H, Pelphrey K, Piven J. Structural and functional magnetic resonance imaging of autism. Int. J. Dev. Neurosci. 2002; 20:421–438. [PubMed: 12175882]

Crackower MA, Oudit GY, Kozieradzki I, Sarao R, Sun H, Sasaki T, Hirsch E, Suzuki A, Shioi T, Irie-Sasaki J, et al. Regulation of myocardial contractility and cell size by distinct PI3K-PTEN signaling pathways. Cell. 2002; 110:737–749. [PubMed: 12297047]

Crawley JN. Designing mouse behavioral tasks relevant to autistic-like behaviors. Ment. Retard. Dev. Disabil. Res. Rev. 2004; 10:248–258. [PubMed: 15666335]

Cross DA, Alessi DR, Cohen P, Andjelkovich M, Hemmings BA. Inhibition of glycogen synthase kinase-3 by insulin mediated by protein kinase B. Nature. 1995; 378:785–789. [PubMed: 8524413]

Crowder RJ, Freeman RS. Phosphatidylinositol 3-kinase and Akt protein kinase are necessary and sufficient for the survival of nerve growth factor-dependent sympathetic neurons. J. Neurosci. 1998; 18:2933–2943. [PubMed: 9526010]

Dakin S, Frith U. Vagaries of visual perception in autism. Neuron. 2005; 48:497–507. [PubMed: 16269366]

Danscher G, Stoltenberg M, Bruhn M, Sondergaard C, Jensen D. Immersion autometallography: histochemical in situ capturing of zinc ions in catalytic zinc-sulfur nanocrystals. J. Histochem. Cytochem. 2004; 52:1619–1625. [PubMed: 15557216]

Dawson GR, Tricklebank MD. Use of the elevated plus maze in the search for novel anxiolytic agents. Trends Pharmacol. Sci. 1995; 16:33–36. [PubMed: 7762079]

de Vries P, Humphrey A, McCartney D, Prather P, Bolton P, Hunt A. Consensus clinical guidelines for the assessment of cognitive and behavioural problems in Tuberous Sclerosis. Eur. Child Adolesc. Psychiatry. 2005; 14:183–190. [PubMed: 15981129]

Dulawa SC, Geyer MA. Effects of strain and serotonergic agents on prepulse inhibition and habituation in mice. Neuropharmacology. 2000; 39:2170–2179. [PubMed: 10963760]

Emamian ES, Hall D, Birnbaum MJ, Karayiorgou M, Gogos JA. Convergent evidence for impaired AKT1-GSK3beta signaling in schizophrenia. Nat. Genet. 2004; 36:131–137. [PubMed: 14745448]

Fombonne E, Roge B, Claverie J, Courty S, Fremolle J. Microcephaly and macrocephaly in autism. J. Autism Dev. Disord. 1999; 29:113–119. [PubMed: 10382131]

Fraser MM, Zhu X, Kwon CH, Uhlmann EJ, Gutmann DH, Baker SJ. Pten loss causes hypertrophy and increased proliferation of astrocytes in vivo. Cancer Res. 2004; 64:7773–7779. [PubMed: 15520182]

Goffin A, Hoefsloot LH, Bosgoed E, Swillen A, Fryns JP. PTEN mutation in a family with Cowden syndrome and autism. Am. J. Med. Genet. 2001; 105:521–524. [PubMed: 11496368]

Groszer M, Erickson R, Scripture-Adams DD, Lesche R, Trumpp A, Zack JA, Kornblum HI, Liu X, Wu H. Negative regulation of neural stem/progenitor cell proliferation by the Pten tumor suppressor gene in vivo. Science. 2001; 294:2186–2189. [PubMed: 11691952]

Hay N. The Akt-mTOR tango and its relevance to cancer. Cancer Cell. 2005; 8:179–183. [PubMed: 16169463]

Jaworski J, Spangler S, Seeburg DP, Hoogenraad CC, Sheng M. Control of dendritic arborization by the phosphoinositide-3′-kinase-Akt-mammalian target of rapamycin pathway. J. Neurosci. 2005; 25:11300–11312. [PubMed: 16339025]

Jiang H, Guo W, Liang X, Rao Y. Both the establishment and the maintenance of neuronal polarity require active mechanisms: critical roles of GSK-3beta and its upstream regulators. Cell. 2005; 120:123–135. [PubMed: 15652487]

Klesse LJ, Parada LF. p21 ras and phosphatidylinositol-3 kinase are required for survival of wild-type and NF1 mutant sensory neurons. J. Neurosci. 1998; 18:10420–10428. [PubMed: 9852579]

Kwon CH, Zhu X, Zhang J, Knoop LL, Tharp R, Smeyne RJ, Eberhart CG, Burger PC, Baker SJ. Pten regulates neuronal soma size: a mouse model of Lhermitte-Duclos disease. Nat. Genet. 2001; 29:404–411. [PubMed: 11726927]

Kwon CH, Zhu X, Zhang J, Baker SJ. mTor is required for hypertrophy of Pten-deficient neuronal soma in vivo. Proc. Natl. Acad. Sci. USA. 2003; 100:12923–12928. [PubMed: 14534328]

Kwon CH, Zhou J, Li Y, Kim KW, Hensley LL, Baker SJ, Parada LF. A neuron-specific enolase-cre line with cre activity in specific neuronal populations. Genesis. 2006; 44:130–135. [PubMed: 16496331]

Li G, Robinson GW, Lesche R, Martinez-Diaz H, Jiang Z, Rozengurt N, Wagner KU, Wu DC, Lane TF, Liu X, et al. Conditional loss of PTEN leads to precocious development and neoplasia in the mammary gland. Development. 2002; 129:4159–4170. [PubMed: 12163417]

Lijam N, Paylor R, McDonald MP, Crawley JN, Deng CX, Herrup K, Stevens KE, Maccaferri G, McBain CJ, Sussman DJ, Wynshaw-Boris A. Social interaction and sensorimotor gating abnormalities in mice lacking Dvl1. Cell. 1997; 90:895–905. [PubMed: 9298901]

Lin CH, Yeh SH, Lin CH, Lu KT, Leu TH, Chang WC, Gean PW. A role for the PI-3 kinase signaling pathway in fear conditioning and synaptic plasticity in the amygdala. Neuron. 2001; 31:841–851. [PubMed: 11567621]

Luikart BW, Nef S, Virmani T, Lush ME, Liu Y, Kavalali ET, Parada LF. TrkB has a cell-autonomous role in the establishment of hippocampal Schaffer collateral synapses. J. Neurosci. 2005; 25:3774–3786. [PubMed: 15829629]

Luo J, Manning BD, Cantley LC. Targeting the PI3KAkt pathway in human cancer: rationale and promise. Cancer Cell. 2003; 4:257–262. [PubMed: 14585353]

Maehama T, Dixon JE. The tumor suppressor, PTEN/MMAC1, dephosphorylates the lipid second messenger, phosphatidylinositol 3,4,5-trisphosphate. J. Biol. Chem. 1998; 273:13375–13378. [PubMed: 9593664]

Manning BD, Cantley LC. United at last: the tuberous sclerosis complex gene products connect the phosphoinositide 3-kinase/Akt pathway to mammalian target of rapamycin (mTOR) signalling. Biochem. Soc. Trans. 2003; 31:573–578. [PubMed: 12773158]

Markus A, Zhong J, Snider WD. Raf and akt mediate distinct aspects of sensory axon growth. Neuron. 2002; 35:65–76. [PubMed: 12123609]

Marui T, Hashimoto O, Nanba E, Kato C, Tochigi M, Umekage T, Ishijima M, Kohda K, Kato N, Sasaki T. Association between the neurofibromatosis-1 (NF1) locus and autism in the Japanese population. Am. J. Med. Genet. B Neuropsychiatr. Genet. 2004; 131:43–47. [PubMed: 15389774]

Mbarek O, Marouillat S, Martineau J, Barthelemy C, Muh JP, Andres C. Association study of the NF1 gene and autistic disorder. Am. J. Med. Genet. 1999; 88:729–732. [PubMed: 10581497]

Moretti P, Bouwknecht JA, Teague R, Paylor R, Zoghbi HY. Abnormalities of social interactions and home-cage behavior in a mouse model of Rett syndrome. Hum. Mol. Genet. 2005; 14:205–220. [PubMed: 15548546]

Moy SS, Nadler JJ, Perez A, Barbaro RP, Johns JM, Magnuson TR, Piven J, Crawley JN. Sociability and preference for social novelty in five inbred strains: an approach to assess autistic-like behavior in mice. Genes Brain Behav. 2004; 3:287–302. [PubMed: 15344922]

Muhle R, Trentacoste SV, Rapin I. The genetics of autism. Pediatrics. 2004; 113:e472–e486. [PubMed: 15121991]

Murcia CL, Gulden F, Herrup K. A question of balance: a proposal for new mouse models of autism. Int. J. Dev. Neurosci. 2005; 23:265–275. [PubMed: 15749251]

Perandones C, Costanzo RV, Kowaljow V, Pivetta OH, Carminatti H, Radrizzani M. Correlation between synaptogenesis and the PTEN phosphatase expression in dendrites during postnatal brain development. Brain Res. Mol. Brain Res. 2004; 128:8–19. [PubMed: 15337313]

Powell CM, Schoch S, Monteggia L, Barrot M, Matos MF, Feldmann N, Sudhof TC, Nestler EJ. The presynaptic active zone protein RIM1alpha is critical for normal learning and memory. Neuron. 2004; 42:143–153. [PubMed: 15066271]

Schumann CM, Hamstra J, Goodlin-Jones BL, Lotspeich LJ, Kwon H, Buonocore MH, Lammers CR, Reiss AL, Amaral DG. The amygdala is enlarged in children but not adolescentswith autism; the hippocampus is enlarged at all ages. J. Neurosci. 2004; 24:6392–6401. [PubMed: 15254095]

Shapiro LA, Ribak CE. Integration of newly born dentate granule cells into adult brains: hypotheses based on normal and epileptic rodents. Brain Res. Brain Res. Rev. 2005; 48:43–56. [PubMed: 15708627]

Soriano P. Generalized lacZ expression with the ROSA26 Cre reporter strain. Nat. Genet. 1999; 21:70–71. [PubMed: 9916792]

Stiles B, Groszer M, Wang S, Jiao J, Wu H. PTENless means more. Dev. Biol. 2004; 273:175–184. [PubMed: 15328005]

Suzuki A, Yamaguchi MT, Ohteki T, Sasaki T, Kaisho T, Kimura Y, Yoshida R, Wakeham A, Higuchi T, Fukumoto M, et al. T cell-specific loss of pten leads to defects in central and peripheral tolerance. Immunity. 2001; 14:523–534. [PubMed: 11371355]

Tang SJ, Reis G, Kang H, Gingras AC, Sonenberg N, Schuman EM. A rapamycin-sensitive signaling pathway contributes to long-term synaptic plasticity in the hippocampus. Proc. Natl. Acad. Sci. USA. 2002; 99:467–472. [PubMed: 11756682]

Waite KA, Eng C. Protean PTEN: form and function. Am. J. Hum. Genet. 2002; 70:829–844. [PubMed: 11875759]

Wiznitzer M. Autism and tuberous sclerosis. J. Child Neurol. 2004; 19:675–679. [PubMed: 15563013]

Yoshimura T, Kawano Y, Arimura N, Kawabata S, Kikuchi A, Kaibuchi K. GSK-3beta regulates phosphorylation of CRMP-2 and neuronal polarity. Cell. 2005; 120:137–149. [PubMed: 15652488]

Zalfa F, Giorgi M, Primerano B, Moro A, Di Penta A, Reis S, Oostra B, Bagni C. The fragile X syndrome protein FMRP associates with BC1 RNA and regulates the translation of specific mRNAs at synapses. Cell. 2003; 112:317–327. [PubMed: 12581522]

Zoghbi HY. Postnatal neurodevelopmental disorders: meeting at the synapse? Science. 2003; 302:826–830. [PubMed: 14593168]

Zori RT, Marsh DJ, Graham GE, Marliss EB, Eng C. Germline PTEN mutation in a family with Cowden syndrome and Bannayan-Riley-Ruvalcaba syndrome. Am. J. Med. Genet. 1998; 80:399–402. [PubMed: 9856571]

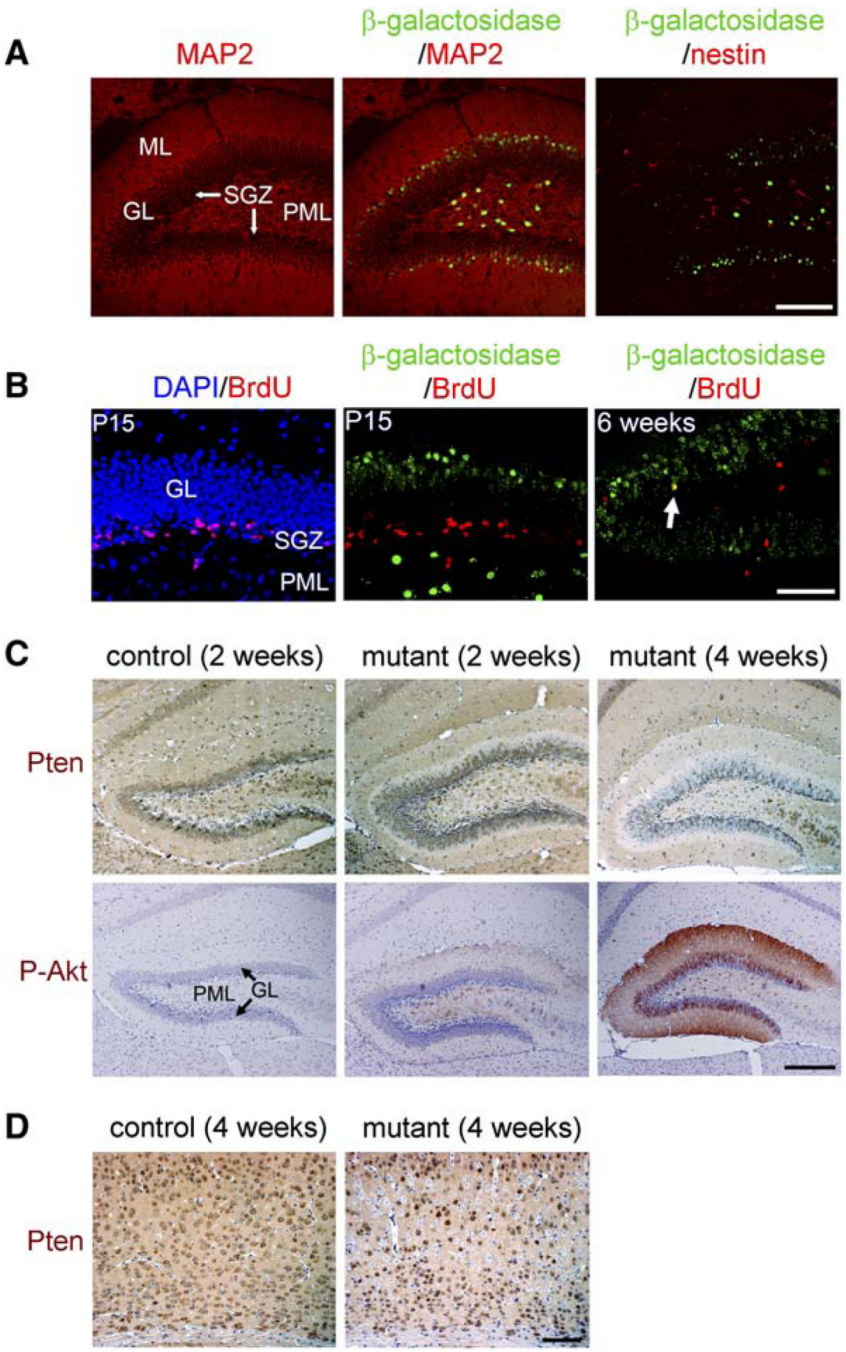

Figure 1. *Pten* Deletion Occurred in Differentiated Neurons

(A) In 2-week-old *Nse-cre; Rosa26R* mice, β-galactosidase signal was detected in MAP2-expressing neurons in the polymorphic layer (PML) and the outer granular layer (GL), close to the molecular layer (ML), in the dentate gyrus, but not in the inner GL, subgranular zone (SGZ), or in cells expressing nestin. Although a similar level and pattern of MAP2 or nestin immunoreactivity appeared in control (either without *cre* or *Rosa26R*), β-galactosidase was not detected (data not shown). Scale bar, 200 μm.

(B) P15 *Nse-cre; Rosa26R* mice injected with BrdU at P14 retained the BrdU signal mainly in the SGZ, which was absent in β-galactosidase-expressing cells in the outer GL and PML. Four weeks after the BrdU injection, BrdU signal was detected in the GL, and some of them

colocalized with β-galactosidase-expressing granule neurons (arrow, for example). Scale bar, 100 μm.
(C) In mutant tissue at 2 weeks of age, similar to β-galactosidase activity in *Nse-cre; Rosa26R* brain, Pten-negative (blue), and P-Akt-positive signals (brown) were detected in the PML and the outer GL. At 4 weeks of age, the number of Pten-negative, P-Akt-positive cells increased in mutant dentate gyrus. Scale bar, 200 μm.
(D) In the sensory cortex layers III to VI, Pten (brown) was detected in most neurons in control. In mutant cortex, Pten-negative cells were mainly detected at layers III to V. Scale bar, 100 μm.

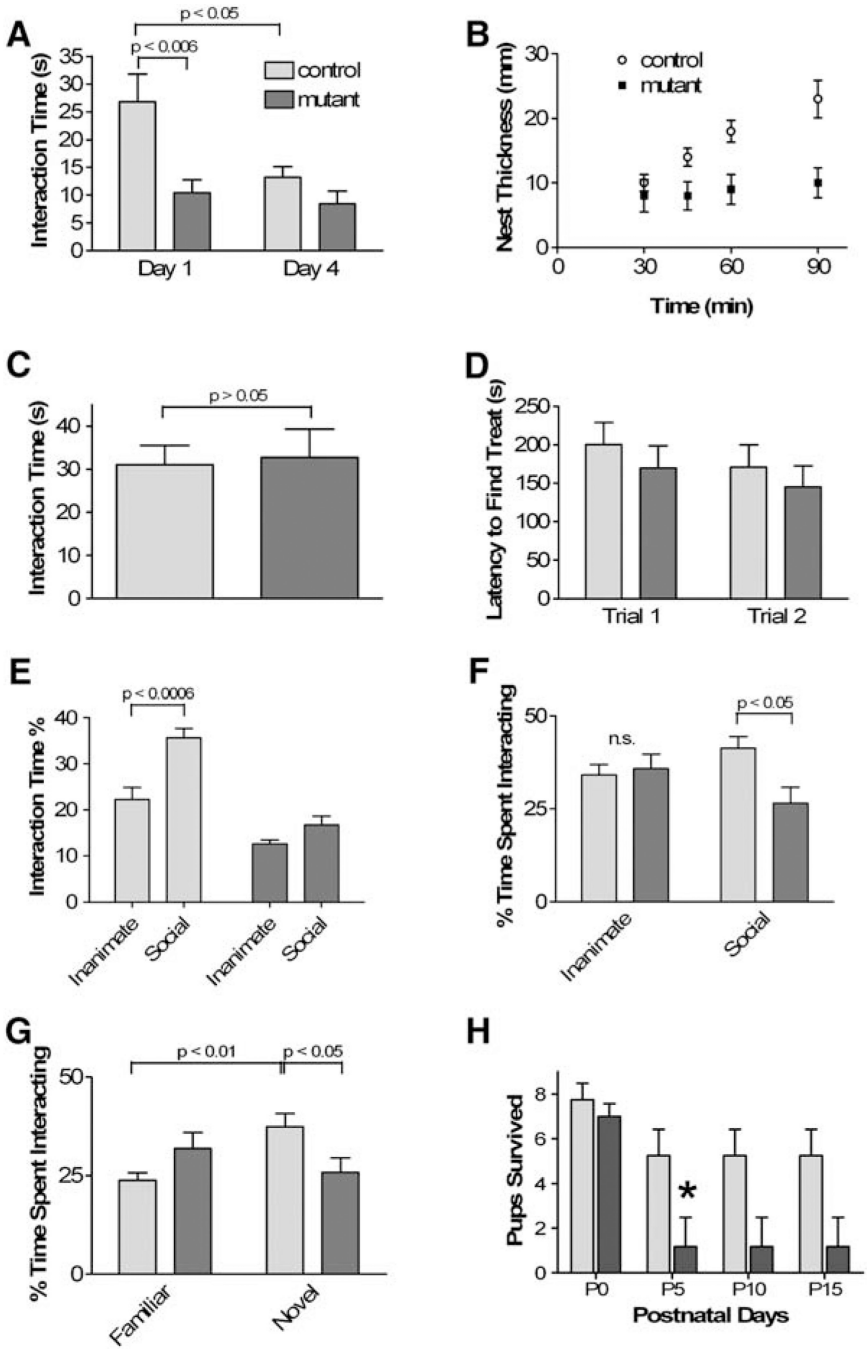

Figure 2. The *Pten* Mutant Mice Were Abnormal in Behavioral Tests for Social Interaction and Social Learning

(A) At day 1, mutants spent significantly less time interacting with a conspecific juvenile compared to controls (n = 12). Control mice spent significantly less time interacting with the same juvenile 3 days hence ($p < 0.05$), yet mutants did not decrease their interaction time ($p = 0.8$). Legend in this panel applies to all bar graphs.

(B) Mutant mice showed significant deficits in nest formation (n = 12). ANOVA revealed a significant effect of genotype ($F_{1,22} = 7.97$, $p = 0.01$), time ($F_{3,66} = 11.37$, $p < 0.00001$), and an interaction between genotype and time ($F^{3,66} = 6.26$, $p < 0.001$).

(C) Time spent interacting with a novel inanimate object under the same conditions as in (A) was not significantly affected by genotype (n = 12).
(D) Mutant mice did not show significant difference from control in latency to find a buried treat following overnight food deprivation (n = 12).
(E) When exposed to caged social and inanimate targets in an open field, controls showed normal preference for a social target over an inanimate target, while mutants spent similar time interacting with both targets (n = 12). Furthermore, mutant mice spent significantly less time interacting with a social target compared to controls ($p < 0.00001$). In this task, there was also a significant decrease in inanimate object interaction time between genotypes ($p < 0.01$), unlike in (C).
(F) In a social preference task, mutants spent less time with a social target compared to controls (n = 12). Time spent with an inanimate object was not significantly different in both groups.
(G) In a preference for social novelty task, controls showed a preference for social novelty, while mutants showed no preference between the social targets (n = 12). Mutants spent significantly less time interacting with a novel social target compared to controls.
(H) Mutant female mice delivered normal-sized pups. Mortality of pups between P0 and P5 was significantly higher in mutants (n = 6) compared to controls (n = 8). *$p < 0.05$ to controls and < 0.005 to P0.

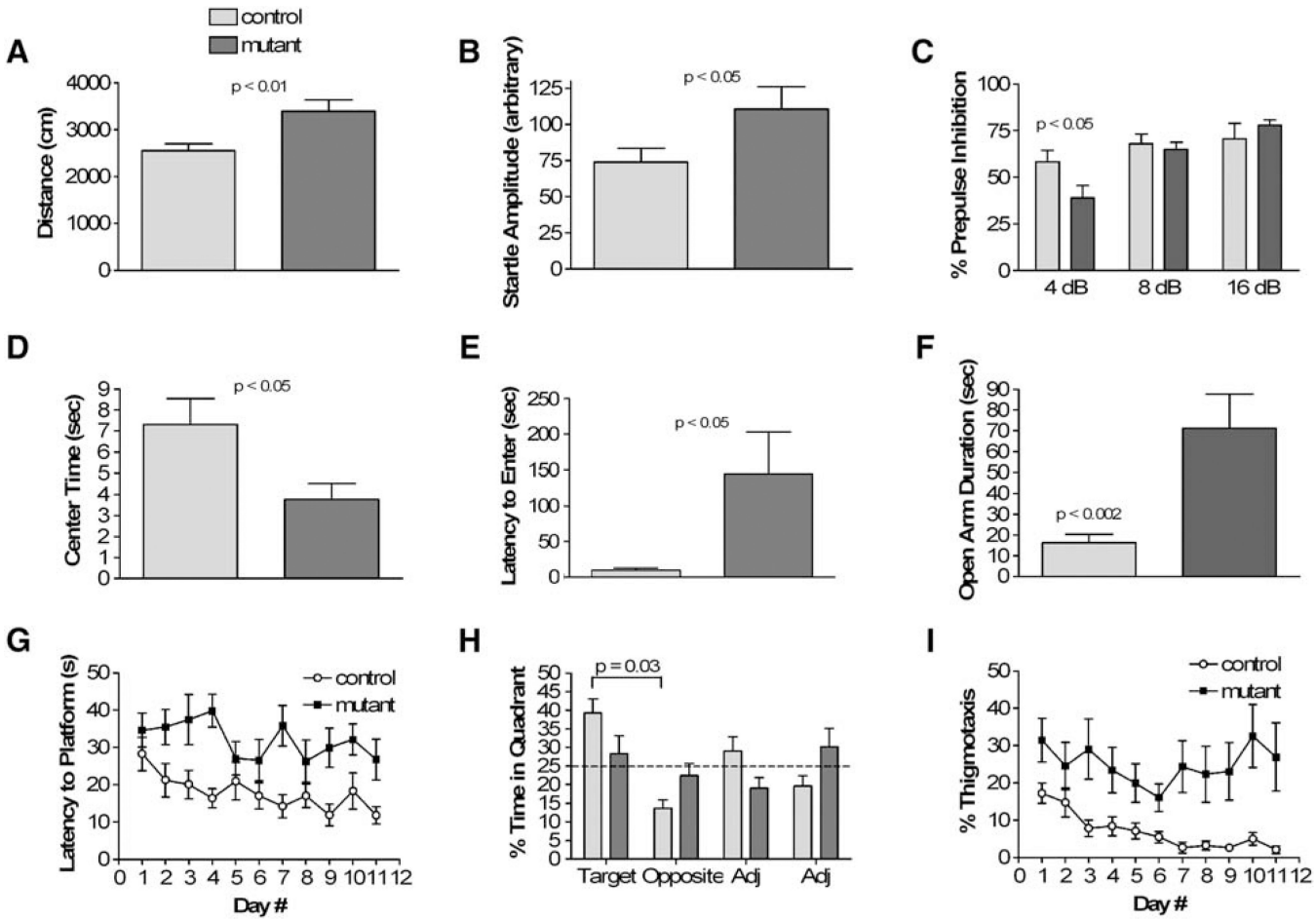

Figure 3. The *Pten* Mutant Mice Showed Abnormalities in Responses to Sensory Stimuli, Anxiety, and Learning

(A) Mutants exhibited increased locomotor activity in an open field test (n = 16 mutants, 17 controls). Average speed was 11.30 ± 0.84 cm/s for mutants and 8.51 ± 0.47 cm/s for controls (p = 0.006). Legend in this panel applies to all bar graphs.

(B) Initial startle response was significantly increased in mutants (n = 11 mutants, 14 controls). Data represent the average startle response to the first six presentations of a 40 ms, 120 dB white noise stimulus.

(C) In a prepulse inhibition test, mutants showed significantly impaired sensorimotor gating (n = 11 mutants, 14 controls).

(D) Mutants exhibited anxiety-like behavior as they spent significantly less time in the center zone of the open field apparatus (n = 16 mutants, 17 controls).

(E) The latency to enter the light side of the dark/light boxes was significantly elevated in mutants (n = 16 mutants, 17 controls).

(F) In elevated plus maze test, mutants exhibited significantly increased duration in open arm (n = 16 mutants, 17 controls).

(G) Mutants exhibited a significantly decreased learning curve in the submerged platform version of the water maze when latency to reach the platform was measured (n = 9 mutants, 12 controls). ANOVA revealed a main effect of genotype ($F_{1,17} = 11.17$, $p < 0.01$) and day number ($F_{10,170} = 2.21$, $p < 0.05$). Similar effect was seen in distance traveled to reach the platform (data not shown). Three mutant mice died during the water maze task due to seizure activity during training.

(H) Controls showed clear preference for target quadrant versus opposite whereas mutants showed no preference (n = 9 mutants, 12 controls).
(I) Mutant mice spent significantly increased time along the edge of the water maze (thigmotaxis, n = 9 mutants, 12 controls). ANOVA revealed a main effect of genotype ($F_{1,17} = 39.76$, $p < 0.00001$).

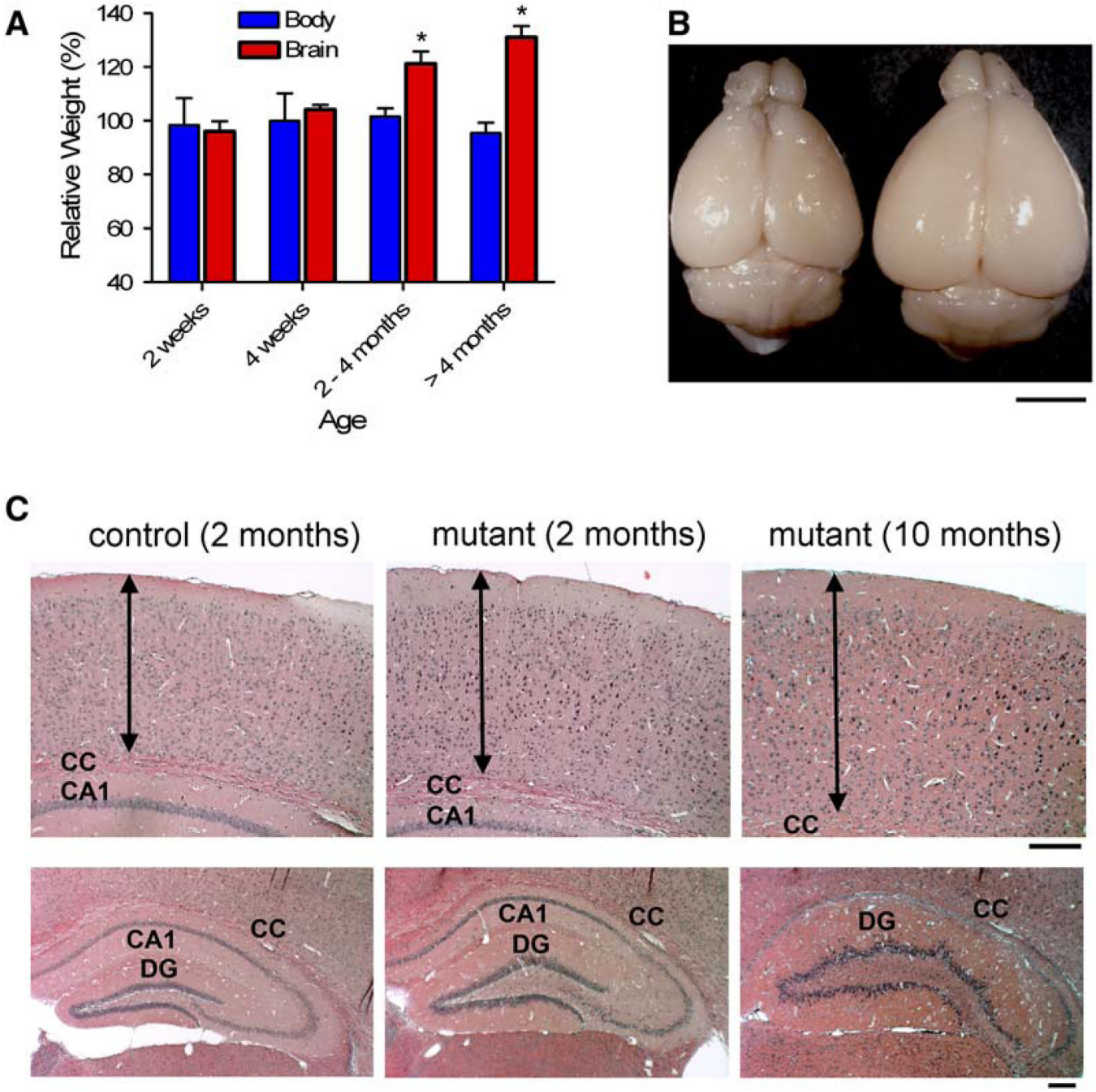

Figure 4. Progressive Macrocephaly and Regional Hypertrophy in the *Pten* Mutant Mice

(A) Relative sizes of mutant brain to control at different ages indicate progressive macrocephaly in mutant mice (n = 4 or more per group). *$p < 0.005$ versus control.

(B) A representative mutant brain at 10 months of age (right) is bigger than that from littermate control. Scale bar, 4 mm.

(C) H/E staining on coronal sections shows that the thickness of the cerebral cortex (arrows), the length between the pial surface and the corpus callosum (CC), increased in adult mutant brain (upper panels). In the hippocampus, progressively enlarged dentate gyri (DG) and compressed or absence of CA1 were seen in mutant brains (lower panels). Scale bars, 200 μm.

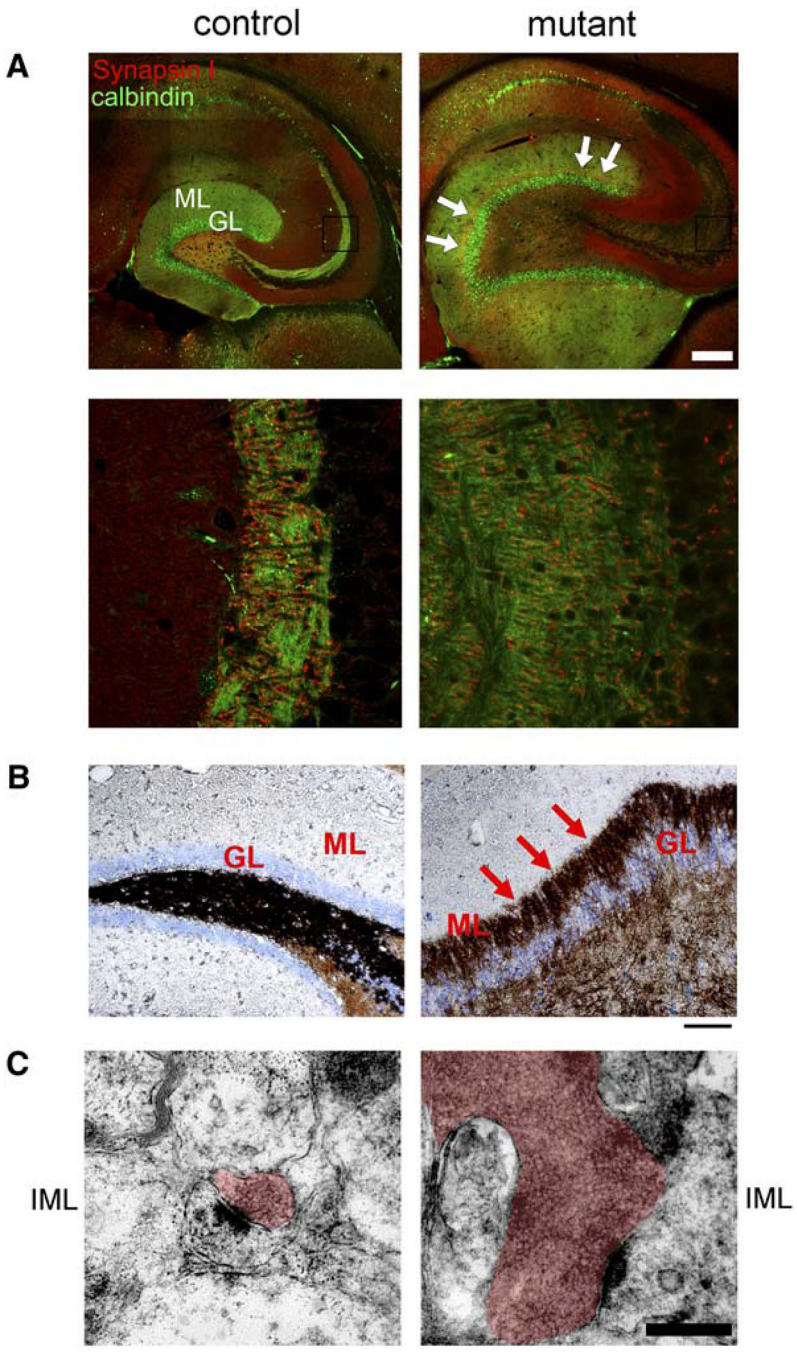

Figure 5. Hypertrophic and Ectopic Axonal Tract with Increased Synapses in *Pten*-Deleted Dentate Gyrus

(A) Horizontal floating sections from 10-month-old brains were stained for synapsin I (red) and calbindin (green). Confocal images showed that elongated and dispersed mossy fiber tract from the granular layer (GL) of mutant dentate gyrus and an ectopic layer of axonal signals (arrows) in the molecular layer (ML), compared to those of control (upper panels). Scale bar, 500 μm. High-magnification images revealed that the mossy fiber synapses spanned a larger area in mutant versus control animals (lower panels; from the boxes in upper panels).

(B) The inner ML of 7-month-old mutant dentate gyrus was positive for Timm staining (arrows), while such signals were absent in control ML. Scale bar, 100 μm.
(C) Electron microscopic analysis of the inner ML (IML) of dentate gyri revealed that the increased axonal staining in mutant was due to enlarged presynaptic varicosities (red highlight). The varicosities of mutant contained a large number of densely packed synaptic vesicles. Scale bar, 0.5 μm.

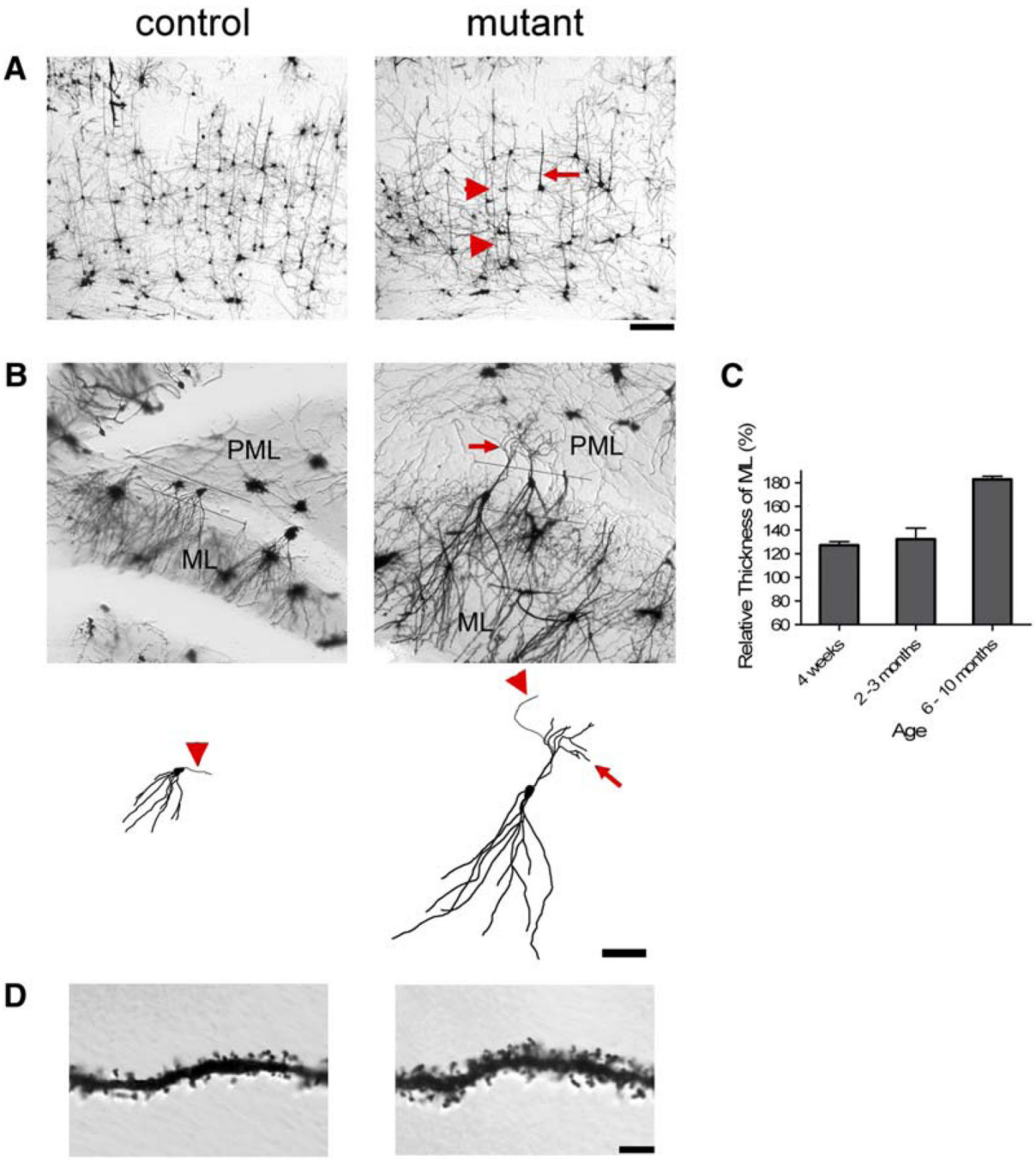

Figure 6. Golgi Stain Revealed Dendritic Hypertrophy, Ectopy, and Increased Spine Density in *Pten*-Deleted Brain

(A) Thickened or elongate neuronal processes (arrow and arrow heads, respectively) were present in mutant cerebral cortex compare to control at 3 months of age. Scale bar, 100 μm. (B) At 8 months of age, increased length of the dendritic arbors in the molecular layer (ML) and ectopic neuronal processes (arrow) in the polymorphic layer (PML) were observed in mutant compare to control (upper panels). Reconstructions of single neurons made from image stacks emphasize the dendritic hypertrophy of the mutant neurons compare to control (lower panels). An axon can be seen emanating from both mutant and control neurons (arrowheads). Scale bar, 100 μm.

(C) Mutant ML was significantly thicker than that of control at all adult ages tested ($p < 0.05$).
(D) Higher-magnification images of dendrites in the ML revealed increased thickness and spine density in mutant (1.434 ± 0.064 spines/μm) versus control (1.077 ± 0.033 spines/μm) brains ($p < 0.000005$, $n = 23$ and 26 dendritic branches from three brains, respectively). Scale bar, 10 μm.

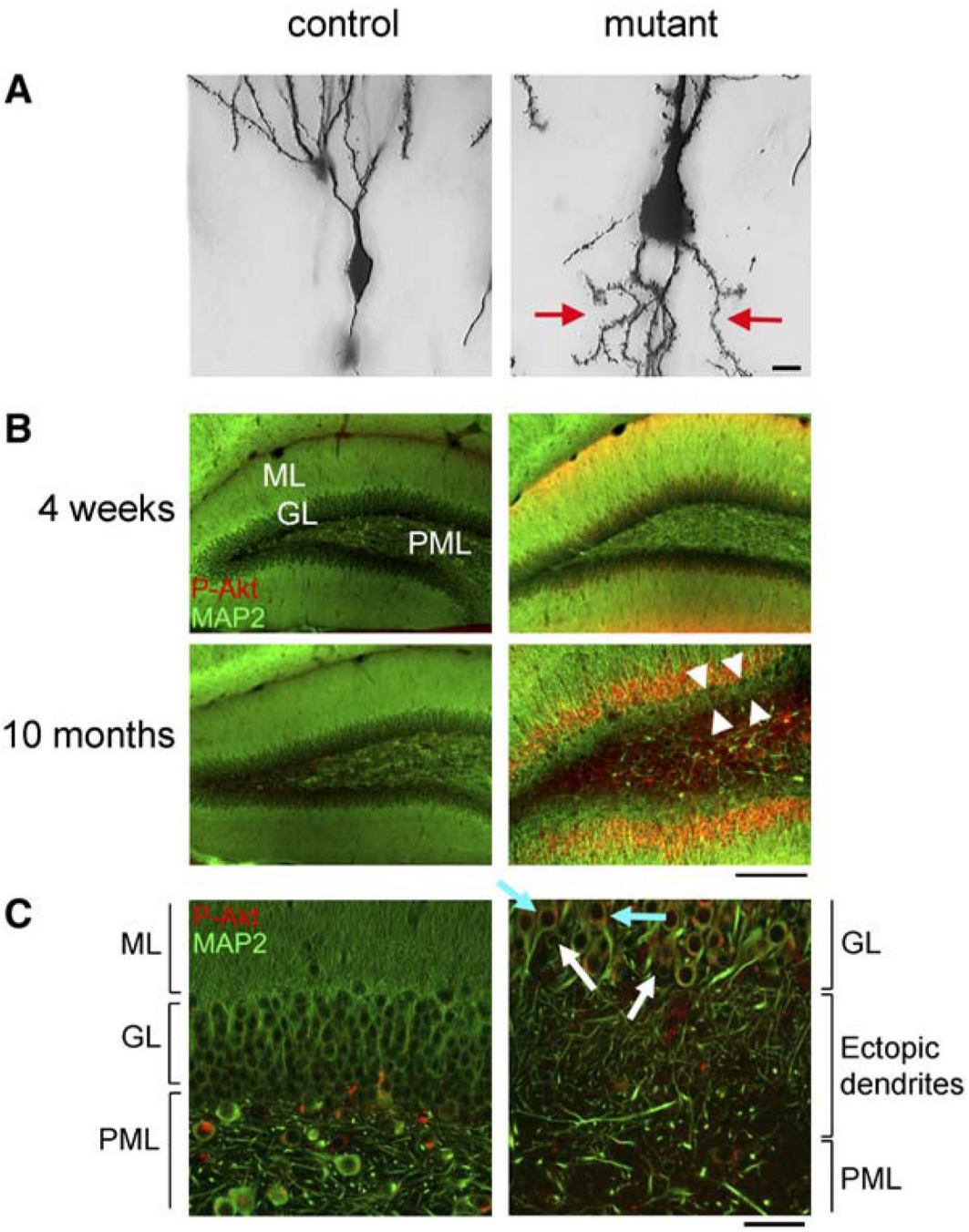

Figure 7. Ectopic Dendrites in *Pten*-Deleted Granule Neurons

(A) High-magnification images on Golgi-stained granule neurons in 8-month-old dentate gyri showed the presence of ectopic, spiny neuronal processes (arrows) in mutant, but not in control. Scale bar, 10 μm.

(B) Coronal floating sections were stained for MAP2 (green) and P-Akt (red). Increased P-Akt was apparent in the granular (GL) and molecular layers (ML) of mutant dentate gyri at all ages, but not in controls. Mutant dentate gyrus at 10 months of age had an ectopic layer of dendrites (arrow heads) between the GL and polymorphic layer (PML), which was absent at 4 weeks of age. Scale bar, 200 μm.

(C) Higher-magnification confocal images revealed that the ectopic dendrites were from P-Akt-positive granule neurons (light blue arrows, for example), but not from P-Akt-negative neurons (white arrows, for example). Scale bar, 50 μm.

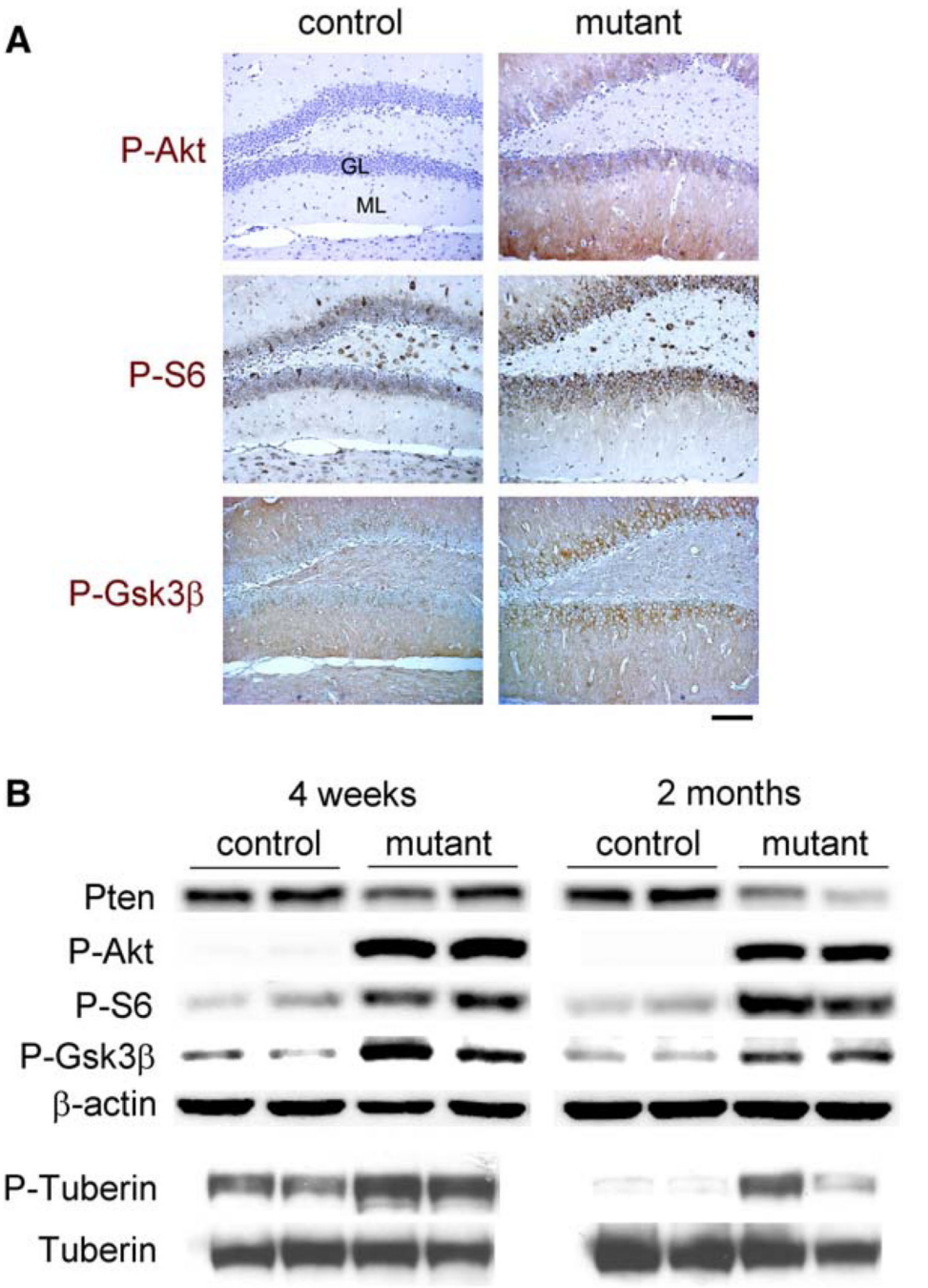

Figure 8. Molecular Signaling Downstream of *Pten*-Deleted Neurons

(A) At 2 months of age, mutant dentate gyri exhibited increased signal (brown) for P-Akt, P-S6 and P-Gsk3β, compared to those in control. The increased staining in mutants was apparent in the granular layer (GL) and inner molecular layer (ML) for P-S6 and in the GL for PGsk3β, whereas both the GL and ML displayed increased P-Akt. All sections were counterstained with hematoxylin, except for P-Gsk3β panels that were stained with methyl green. Scale bar, 200 μm.

(B) Western blot analysis showed decreased Pten and increased P-Akt, P-S6, P-Gsk3β, and P-Tuberin in mutant versus control at all ages tested. $p < 0.005$ for Pten at 2 months and P-Akt; $p < 0.1$ for P-S6, P-Gsk3β and P-Tuberin.